Preparation Of Nano Pore MOR Membranes: Experimental, Modeling And Simulation

Mansoor Kazemimoghadam, Zahra Amiri-Rigi

Department of Chemical Engineering, Malek-Ashtar University of Technology, Tehran, Iran
Department of Chemical Engineering, South Tehran Branch, Islamic Azad University, Tehran, Iran
mzkazemi@gmail.com

Abstract: Nano pore Mordenite membranes were prepared on the outer surface of ceramic tubular tubes via hydrothermal synthesis and evaluated for dehydration pervaporation of water unsymmetrical dimethyl hydrazine UDMH mixtures. Highly water-selective mordenite membranes were prepared and the optimum reaction condition was found to be 24 h crystallization time and 170oC crystallization temperature. Effect of gel composition on separation factor and water flux of the water-UDMH mixtures was investigated. X-ray diffraction (XRD) patterns showed that mordenite is the only zeolite material which presents in the membrane. Morphology of the supports subjected to crystallization was characterized by Scanning Electron Microscopy (SEM). In PV of the water-UDMH mixtures, the membrane exhibits a hydrophilic behavior, with a high selectivity towards water and a good flux. The best membranes had a water flux of 2.67 kg/m2.h at 27oC. The best PV selectivity was obtained to be 264. A comprehensive, unsteady state model was also developed for pervaporation of water-UDMH mixture by COMSOL Multiphysics 5.2 software, based on solving continuity and momentum equations simultaneously. COMSOL solves Navier-Stokes equations by finite element method (FEM). The 2D model was capable of predicting concentration in feed and membrane sections and velocity distribution in feed compartment.

Keywords: Nano pore Zeolite membrane; Mordenite; Pervaporation; UDMH; hydrothermal synthesis; Modeling.

1. Introduction

UDMH is an important liquid propellant; however it also finds many new applications as an oxygen scavenger for boiler-feed water, a starting material for drug and dye intermediates, a catalyst for polymerization reactions, etc. [2-6]. Membrane-based PV technology has all the requirements for completely replacing extractive distillation for separation of the azeotropes. This can be combined with simple distillation as a hybrid process for enrichment of UDMH to high purity levels. PV is an economical separation technique compared to conventional separation methods such as distillation, especially in processes involving azeotropes, isomers and removal or recovery of trace substances. Due to its high separation efficiency and flux rate, PV results in energy cost saving and safe operation [7]. Removal of organic compounds from aqueous solutions is important for the recovery of valuable organic products and highly hazardous materials, for the recycling of process water and for the treatment of waste water [8, 9]. Generally, distillation can be used to remove organic compounds from water. However, for low organic concentrations or thermally sensitive organic compounds, distillation is neither economical nor suitable. Furthermore, PV has several advantages over traditional distillation: (1) reduced energy demand, because only a fraction of the liquid that needs to be separated is vaporized, (2) simple equipment, since only a vacuum pump is used to create the required driving force and (3) lower capital cost [10, 11]. Thus, relatively mild operational conditions and high effectiveness make PV an appropriate technique for such separations. Most PV studies have been recently focused on dehydration of organic mixtures [12-22]. Dehydration of hydrazine and monomethylhydrazine (MMH) using ethyl cellulose membranes have been previously carried out [8, 6, 23, 24]. However, ethyl cellulose cannot be used to dehydrate UDMH because it is degraded rapidly. Also, hydrophobic polymers such as poly (dimethelsiloxane) (PDMS) cannot withstand the highly alkaline (pH=13-14) medium, whereas membranes made of polyethylene and polypropylene give negligible flux so that UDMH cannot be selectively extracted from its dilute reaction liquor. The problem of chemical compatibility is also encountered in the case of hydrophilic polymers such as poly (vinyl alcohol) and poly (acrylic acid) [3-5]. Chitosan, a derivative of the naturally abundant biopolymer chitin, is fully stable in anhydrous UDMH and hence can be selected for its dehydration, keeping in mind its highly hydrophilic nature and good mechanical strength. The promising potential of chitosan as a PV membrane has already been exploited for dehydration of alcohols such as ethanol and isopropanol. This polymer has recently been used to form selective and permeable blend membranes with poly (vinyl alcohol), sodium alginate, etc. However, unfortunately polymeric membranes behaved unsuitable in terms of selectivity and flux in general for water-UDMH mixtures (selectivity and flux of about 10 and 0.01 kg/m^2.h, respectively) [23-26]. However, there has been an increasing interest towards zeolite membranes due to their strong potential in separation of liquid mixtures by PV. Zeolite membranes can be prepared with different methods: in situ hydrothermal synthesis; chemical vapor phase method, spray seed coating, etc. Whatever the method, an inorganic porous support is required and its nature and structure may affect the quality of the composite zeolite membrane. A popular support is made of sintered alumina. Nevertheless, this support is expensive and makes the membranes uneconomical. It is thus important to study the possibility of obtaining membranes with chip supports. Considering its abundant resource, its low cost and its easy processing into a support with a regular structure by sintering, kaolin is a good candidate for the zeolite membranes. Dehydration of organic solvents is presently the major market of PV. Zeolite NaA membranes were reported to be excellent materials for solvent dehydration by PV. But under slightly harsh conditions and under hydrothermal stresses, zeolite NaA membranes turn out to be unstable due to hydrolysis. There are only a few attempts to develop hydrophilic highly siliceous zeolite membranes of different Si/Al ratios with improved hydrothermal stabilities [27-31]. In pervaporation, the feed mixture is contacted with a nonporous perm selective membrane. Separation is, in general, explained by the steps of sorption into, diffusion through and desorption from the membrane. The latter is usually considered to be fast and taking place at equilibrium, while diffusion is

kinetically controlled and the slowest step of the process. Permeation is dependent on sorption and diffusion steps. The driving force for the separation is created by maintaining a pressure lower than the saturation pressure on the permeate side of the membrane. Many studies have been carried out to simulate mass transfer through PV membranes [8, 22, 32-37]. The mechanism of separation is usually explained in terms of sorption-diffusion processes [1, 38-41]. Mass transfer through PV membranes is usually described by the equations of mass and momentum conservation (Navier-Stokes equations). Modeling based on solving these equations with finite element method (FEM) is widely used to describe concentration distribution in PV systems [32]. Based on this method, Moulik et al. proposed a steady state model to predict mass transfer of MMH and UDMH solutions by pervaporation [8]. Their results were in good agreement with experimental data. However, their model was not comprehensive, since they only modeled the membrane section of the module and also assumed the conditions to be steady state. As understood, a complete transient model is essential that is capable of modeling membrane section as well as feed compartment. Since stability of the zeolites in the harsh environments enhances with its silica content, in this paper, preparation method of the hydrophilic mordenite zeolite membrane on mullite support was reported. Performance of the membrane prepared by hydrothermal in situ crystallization was studied for separation of the water–UDMH mixtures by PV through the membrane nano-pores. Then a comprehensive model was developed taking into account the time dependency of the concentration distribution, which was neglected in previous studies. Thus an unsteady state 2D model was developed based on solving Navier-Stokes equations of mass and momentum transfer simultaneously in the feed side of the membrane system. The concentration distribution of water in membrane side of the separation module was also obtained by solving continuity equation.

2. Experimental

In this research, mullite supports were prepared from kaolin clay. Kaolin clay is thermally converted to mullite via high temperature calcinations. The mullitization reaction takes place when kaolin clay is utilized as the sole source of silica and alumina. The kaolin material used in this study (SL-KAD grade) was obtained from WBB cooperation. UDMH (98%) and Sodium hydroxide (Merck) were also used in all experiments. Cylindrical shaped (tubular) bodies were conveniently made by extruding a mixture of about 67-75% kaolin clay and 25-33% distilled water using an extruder. Suitable calcination temperatures and periods are those at which the clay converts to mullite and free silica. Good results were achieved by calcinations for about 3 h at a temperature of about 1250^{o}C. Support preparation method was published in details elsewhere [42]. The mordenite zeolite membranes were synthesized on the outer surface of the porous mullite tubes. The Si source was sodium silicate and the Al source was sodium aluminate. Synthesis solution was prepared by mixing aluminate and silicate solutions. NaOH was dissolved in distilled water. The solution was divided into two equal volumes and kept in polypropylene bottles. Aluminate solution was prepared by adding sodium aluminate to one part of the NaOH solution and was mixed until cleared. Silicate solution was prepared by adding sodium silicate to another part of the NaOH solution. It was then poured into aluminate solution and well mixed until a thick homogenized gel was formed. Molar composition of the starting gel of the mordenite zeolite membranes was SiO_2/Al_2O_3=9–30, Na_2O/SiO_2=9.75, H_2O/Na_2O=780. Fig. 1 shows a schematic representation of mordenite structure.

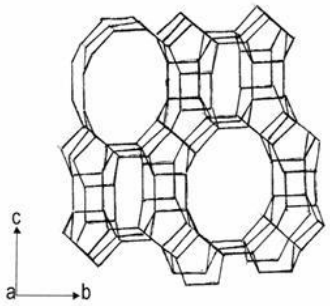

Fig. 1 *Schematic representation of mordenite structure*

For membrane preparation, two ends of the supports were closed with rubber caps to avoid any precipitation of the zeolite crystals on the inner surface of the supports during membrane synthesis. The seeded supports were placed vertically in a Teflon autoclave. The solution was carefully poured into the autoclave and then the autoclave was sealed. Crystallization was carried out in an oven at a temperature of 170°C for 24 h. Then, the samples were taken and the synthesized membranes were washed several times with distilled water. The samples were then dried at room temperature in air and then dried in the oven at 100°C for 15 h prior to characterization and evaluation [43, 1]. The zeolite membranes were used for dehydration of water-UDMH mixtures. The experiments were carried out at a temperature of 30°C and a pressure of 1.5 mbar at the permeate side, within a period of 30-60 min. The final membrane used for PV experiments had 44 cm^2 surface area, 12 cm length, 5 mm inner radius and 5.835 mm outer radius. The feed solution flowed over the outer surface of the membrane module and the permeate water was collected from the inner part of that. Permeate concentrations were measured using GC (TCD detector, Varian 3400, carrier gas: hydrogen, column: polyethylene glycol, sample size: 5 µm, column and detector temperatures: 120-150°C, detector flow: 15 ml/min, carrier flow: 5 ml/min, column pressure: 1.6 kpa, GC input pressure: 20 kpa). Performance of PV was evaluated using values of total flux ($kg/m^2.h$) and separation factor (dimensionless). While PV system was at steady state (after 20 min), weight of permeate was measured at 30 min period and then flux was obtained. The change in feed concentration due to permeation was negligible because the amount of permeate was small (max 2 ml) compared with total liquid volume in the system (0.5 lit). A three stage diaphragm vacuum pump (Vacuubrand, GMBH, Germany) was employed to evacuate the permeate side of the membrane to a pressure of approximately 1.5 mbar, while the feed side was kept at atmospheric pressure. The permeate side was connected to a liquid nitrogen trap via a hose to condense the permeate (vapor) (Fig. 2).

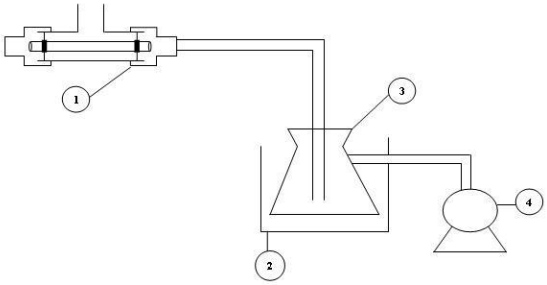

Fig. 2 *PV setup; 1- feed container and PV cell 2- liquid nitrogen trap 3- permeate container 4- three stage vacuum pump*

Phase identification was performed by XRD (Philips PW1710, Philips Co., Netherlands) with CuKα radiation. In addition, morphological studies were performed using SEM (JEM-1200 or JEM-5600LV equipped with an Oxford ISIS-300 X-ray disperse spectroscopy, EDS).

3. Modeling

Fig. 3 represents the schematic diagram of the model domain used in the simulation. Feed solution containing a mixture of 5 wt. % UDMH and 95 wt. % water flows tangentially through the upper side of the membrane system (z=0). The feed exits from the upper side of the feed section and recirculates inside the system ($r=R_3$). The membrane at z=H (membrane height) is closed.

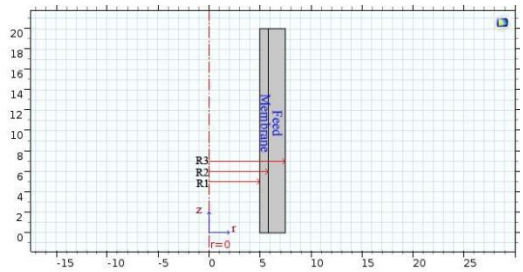

Fig. 3 *Schematic diagram of model domain used for simulation*

The main assumptions to develop the numerical simulation are as follows:

- Unsteady state and isothermal conditions.
- No chemical reaction occurs in feed stream.
- Feed solution flows only in the z direction.
- Laminar feed flow in the membrane system.
- Thermodynamic equilibrium considered at the interface of feed and membrane.
- Small amount of UDMH permeates through the membrane.
- Mass transfer resistance of the support layer was assumed to be negligible.
- Fouling and concentration polarization effects on the PV of UDMH solution are negligible.
- The fluid is incompressible.
- Feed viscosity is constant.

Although the diffusive mass transfer in the direction of flow (z direction) is small due to convective flux in this direction, it is not neglected compared to diffusive mass transfer in the r direction. Therefore, axial and radial diffusions inside the membrane and feed phase are considered in the continuity equations. Moreover, the small permeation of UDMH through the membrane is considered in the simulation by applying selectivity equation (Eq. (1)). The penetration of UDMH through the selective membrane is described by the following equation:

$$S = \frac{x_{UDMH}}{x_{water}} \times \frac{y_{water}}{y_{UDMH}} \quad (1)$$

The concentration of UDMH in the permeate side (y_{UDMH}) must be determined by trial and error method. In this method, an initial value for y_{UDMH} is guessed. Then the water concentration in the permeate side is calculated using model equations. This calculated value then is compared with the guessed value. If the difference between the old and new values is less than a determined error, the guessed UDMH concentration is considered as the correct concentration. Otherwise, another guess must be made for y_{UDMH}. Mass transport in the membrane system is described using continuity equation. The following equation presents the differential form of this equation [45]:

$$\frac{\partial C_{water}}{\partial t} + \nabla.(-D_{water}\nabla C_{water} + U.C_{water}) = R \quad (2)$$

Where C_{water} denotes water concentration (mol/m^3), D_{water} denotes water diffusion coefficient (m^2/s), U denotes the velocity vector (m/s) and R denotes the reaction term (mol/m^3.s). Since no chemical reactions takes place in UDMH/water PV, the reaction term is zero. Continuity equation was defined and solved in COMSOL Multiphysics 5.2 by adding a "transport of diluted species" physic to the model. Velocity distribution was obtained by solving Navier-Stokes equation for momentum balance, simultaneously with continuity equation in the feed side. This was done by adding a "laminar flow" physic to the whole model in COMSOL Multiphysics 5.2. The following equation describes the momentum conservation equation [44]:

$$\rho\frac{\partial u}{\partial t} + \rho(u.\nabla)u = \nabla.[-P + \mu(\nabla u + (\nabla u)^T)] + F \quad (3)$$

$$\nabla.(u) = 0 \quad (4)$$

Where u denotes z-component of velocity vector (m/s), ρ denotes feed density (kg/m^3), P denotes pressure (Pa), μ denotes feed viscosity (Pa.s) and F denotes a body force (N).

3.1. Feed phase simulation

By applying mentioned assumptions to the Eq. (2), unsteady state form of the continuity equation for water mass transport in the feed side is obtained:

$$\frac{\partial C_{water}}{\partial t} - \frac{1}{r}\frac{\partial}{\partial r}\left(D_{water} r \frac{\partial C_{water}}{\partial r}\right) - \frac{\partial}{\partial z}\left(D_{water}\frac{\partial C_{water}}{\partial z}\right) + u\frac{\partial C_{water}}{\partial z} = 0 \quad (5)$$

The simplified form of the momentum transport equations considering above assumptions will be as follows:

$$\rho\left(\frac{\partial u}{\partial t} + u\frac{\partial u}{\partial z}\right) - \frac{1}{r}\frac{\partial}{\partial r}\left(r\mu\frac{\partial u}{\partial r}\right) - \frac{\partial}{\partial z}\left(\mu\frac{\partial u}{\partial z}\right) = -\frac{\partial P}{\partial z} \quad (6)$$

$$\frac{\partial u}{\partial z} = 0 \quad (7)$$

r and z denote radial and axial coordinates, respectively.

The initial conditions for mass and momentum conservation equations are as follows:

at t=0, $C_{water\text{-}feed}=C_{0,water}$ and $u=u_0$ (8)

Where $C_{water\text{-}feed}$ is water concentration in feed phase, $C_{0,\ water}$ is its initial value and u_0 is initial velocity of feed flow.

The boundary conditions for mass conservation equations in feed phase are as follows:

at z=H, $\frac{\partial C_{water-feed}}{\partial z}=0$ (Insolation boundary) (9)

at z=0, $C_{water\text{-}feed}=C_{0,water}$ (Inlet boundary) (10)

The convective flux boundary condition is assumed at $r=R_3$:

at $r=R_3$, Convective flux (11)

The convective flux boundary condition assumes that all mass passing through this boundary is controlled by convection mechanism. Thus, mass transport due to diffusion is zero at this boundary [32].

At the interface of membrane-feed, the equilibrium condition is assumed:

at r= R_2, $C_{water-feed}=\frac{C_{water-membrane}}{n}$ (12)

In which $C_{water\text{-}membrane}$ is water concentration in membrane section and n is partition coefficient obtained from selectivity equation as follows:

$$n=\frac{y_{UDMH}}{x_{UDMH}}\times S=\frac{C_{water-membrane}}{C_{water-feed}} \quad (13)$$

As mentioned earlier, permeate concentration of UDMH must be obtained using trial and error method, and then is placed in the above equation. The boundary conditions for momentum transfer equation are as follows:

at z=0, $u=u_0$, (Inlet boundary) (14)

At the outlet, the pressure is atmospheric pressure:

at $r=R_3$, $P=P_{atm}$, (Atmospheric pressure) (15)

At $r=R_2$ and z=H, u=0 (No slip condition) (16)

3.2. Membrane phase simulation

Mass transport of water in membrane is controlled only by diffusion mechanism. Therefore, the unsteady state continuity equation for water can be written as:

$$\frac{\partial C_{water-membrane}}{\partial t}-\frac{1}{r}\frac{\partial}{\partial r}\left(D_{membrane}r\frac{\partial C_{water-membrane}}{\partial r}\right)-\frac{\partial}{\partial z}\left(D_{membrane}\frac{\partial C_{water-membrane}}{\partial z}\right)=0 \quad (17)$$

where $M_{embrane}$ is water diffusion coefficient in membrane (m^2/s).

Membrane phase boundary conditions are given as:

at $r=R_2$, $C_{water-membrane}=n\times C_{water-feed}$ (Equilibrium condition) (18)

at r= R_1, $C_{water-membrane}=0$ (Dry membrane condition) (19)

at z=0 and z=H, $\frac{\partial C_{water-membrane}}{\partial z}=0$ (No flux condition) (20)

At the permeate-membrane interface, water concentration assumed to be zero due to the vacuum applied.

3.3. Numerical solution of conservation equations

Set of model equations, including mass and momentum transfer equations in the membrane module along with suitable boundary conditions was solved using COMSOL Multiphysics software version 5.2. Finite element method (FEM) is used by this software to solve conservation equations numerically. Previous simulations of membrane separation processes using FEM showed that this method is an accurate, valid and powerful technique for solving mass and momentum equations [8, 32, 36, 45, 46]. The computational time for solving the equations was about 900s. For meshing, we started with coarser meshes (with triangular elements). This was done automatically with COMSOL software. With selecting finer meshes, better results were obtained. At last, we used extra fine mesh, consisted of 72777 domain elements and 2020 boundary elements for solving the set of equations. Fig. 4 represents the meshes created by COMSOL Multiphysics 5.2 software. Due to considerable difference between z and r dimensions, a scaling factor equal to 6 was used in z direction. Therefore, the results were reported in dimensionless height.

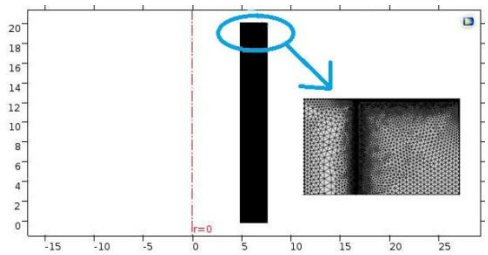

Fig. 4 *Magnified segment of the meshes used in the modeling*

4. Results and discussion

4.1. XRD patterns and SEM photographs of mordenite membrane

It is well known that PV performance of a dense polymeric membrane depends on the ability of solvent species to be dissolved in the membrane at its interfaces, and their diffusion into the membrane. When a zeolite membrane is used as separation barrier, the solvent species cannot be dissolved in the membrane phase but they are adsorbed on zeolite sites of the inorganic materials. Their adsorbed capacities depend on the affinity of membranes towards the solvents to be removed. The membrane exhibited a high selectivity towards water in the water-UDMH mixtures. The results showed that the permeate water flux reaches to a value as high as 2.67 $kg/m^2.h$ for a UDMH concentration of 5 wt. %. The fact that the membrane has a high selectivity to water clearly indicates that the zeolite layer does not have any through-holes, and the transport is diffusive but not convective. The results also confirm that the mordenite membrane behaves as a hydrophilic membrane, probably due to the presence of polar Al atoms in the zeolite crystal structure. The mordenite membrane has large channels of 0.67 nm × 0.70 nm and small channels of 0.26 nm × 0.56 nm, making the mordenite membrane suitable for removing water from organics. The mordenite membrane showed a water-UDMH ideal selectivity of 264 at 27°C, indicating its reasonable quality. Even higher selectivity's may be expected for higher quality membranes. The kinetic diameter of water is 0.26 nm. During PV, water permeates through both zeolite and non-zeolite pores because of its higher diffusion rate through the membrane nano-pores.

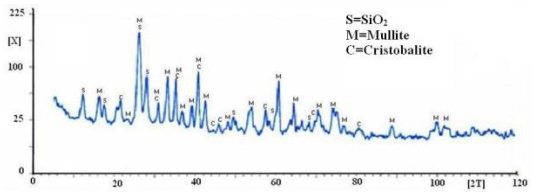

Fig. 5 *XRD pattern of the mullite support*

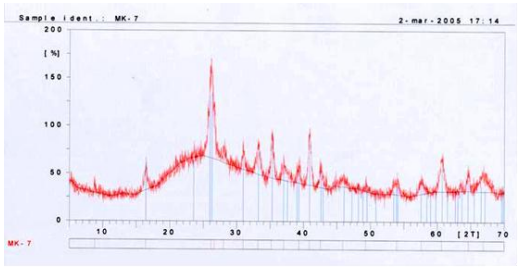

Fig. 6 *XRD pattern of the mordenite zeolite membrane*

Fig. 5 and 6 show XRD patterns of the mullite support and the mordenite zeolite membrane. Morphology of the support subjected to crystallization was characterized by SEM (Fig. 7).

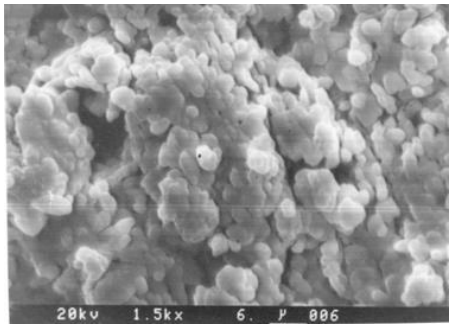

Fig. 7 *SEM of the mullite support*

a) surface *b) cross section*

Fig. 8 *SEM of the mordenite zeolite membranes*

Fig. 8 shows the morphology of the mordenite membrane (surface and cross section). As seen, most of the crystals lie disorderly on the surface. The SEM photograph of the mordenite membrane (cross section) shows that the mullite surface is completely covered by a mordenite crystal layer, whose thickness is larger than 40 µm. The crystal layer is composed of two layers, the top layer consists of pure mordenite crystals and the intermediate one, of mordenite crystals grown in the mullite pores. As can be seen in Table 1, the best selectivity was 264 and the best water flux was 2.67kg/m^2.h at 27^{o}C. The best membranes were prepared using the following gel molar composition: 9.75Na_2O: 1.0Al_2O_3: 9.0SiO_2: 780H_2O. Also, it was found that water separation factor increases with decreasing the SiO_2/Al_2O_3 ratio.

Table 1 *Flux and separation factor of the mordenite zeolite membranes*

No	Na_2O/Al_2O_3	SiO_2/Al_2O_3	H_2O/Al_2O_3	T (h)	T (°C)	UDMH (%)	Flux (kg/m^2.h)	Separation factor
1	9.75	30	780	24	170	5	2.67	132
2	9.75	17	780	24	170	5	0.94	198
3	9.75	9	780	24	170	5	2.14	264

4.2. Water concentration distribution in feed phase

Fig. 9 shows the concentration distribution of water in feed phase at different separation times. The UDMH/water solution containing 95 wt. % water flows over the outer surface of the membrane module (z=0). At z=0, the water concentration is maximum (95 wt. %). As the feed solution flows in the feed compartment, water moves towards the membrane surface due to the concentration and pressure differences (driving forces). Therefore, the water concentration on the membrane surface is less than its value at feed bulk (where water concentration is equal to its initial value, $C_{0,\ water}$). The water concentration on the membrane surface was indicated by the membrane selectivity (Eq. 1) and its value in the membrane side. Since water concentration in membrane is always less than its value in feed, the water concentration on membrane-feed boundary ($r=R_2$) is always less than its value in feed bulk. By increasing the time of separation process, water concentration in concentrate part (feed part) decreases due to the water diffusion through the membrane. Fig. 10 presents the water concentration in the feed phase versus r-coordinate at different heights and times. As can be seen from the figure, with increasing height of the membrane module, total concentration decreases. This is because of more mass transfer towards the membrane at the regions near the feed inlet, due to greater concentration gradients as driving forces, which results in less total concentrations at higher heights. Water concentration increases along r direction, as expected. The concentration gradient is great at regions near the membrane-feed interface ($r=R_2$) due to the mass transfer towards the membrane at this region. In higher heights however, the concentration gradient along r direction decreases. This can be attributed to less concentrations and velocities in regions near z=H compared to feed inlet, as mentioned before, which reduce the driving force (concentration gradient). Over an extended period of time, total concentration decreases due to mass transfer through the membrane. At 5mm and 10mm heights, the water concentration reached a constant value at 1200s, so that it didn't decrease with time. This is exactly in agreement with what we reported in the experiments.

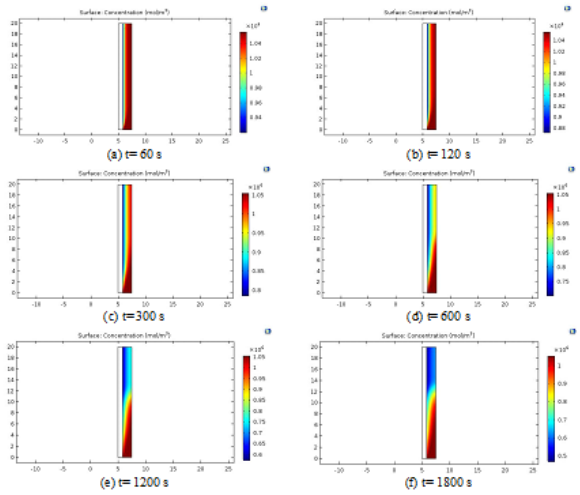

Fig. 9 *Concentration distribution of water in feed phase ($C_{water\text{-}feed}$) at different times (1 l/min flow rate and 30°C temperature); (a) 60s, (b) 120s, (c) 300s, (d) 600s, (e) 1200s and (f) 1800s*

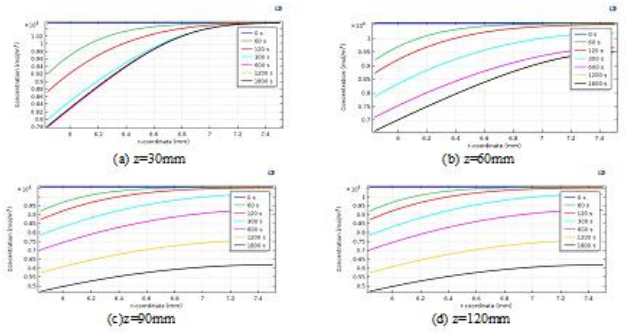

Fig. 10 *Concentration distribution of water in feed phase ($C_{water\text{-}feed}$) vs. radius at various membrane heights (1 l/min flow rate and 30°C temperature): (a) 30mm, (b) 60mm, (c) 90mm and (d) 120mm*

Fig 11 demonstrates the concentration distribution along z coordinate at constant flow rate (1 l/min) and different radii.

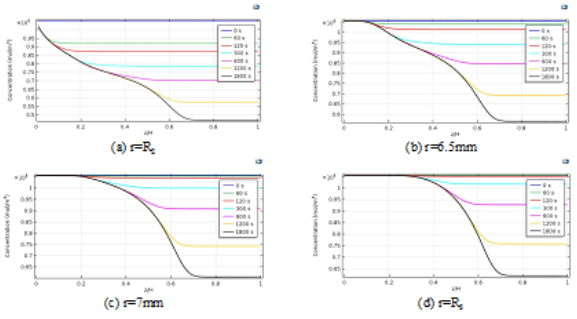

Fig.11 *Water concentration distribution in feed phase vs. dimensionless height (1 l/min flow rate and 30°C temperature) at various radii; (a) r=R_2, (b) r=6.5mm, (c) r=7mm and (d) r=R_3*

Results show that the variation of water concentration along the z coordinate is considerable and cannot be neglected compared to its variation along r coordinate. The figure also indicates that the concentration gradient near the membrane-feed interface (r=R_2) is greater, while is delayed at greater radii. This behavior is due to the diffusion of water through the membrane at this region. Concentration variation increases over an extended period of time. Thus, time-dependent study is necessary in PV simulations and the stationary condition which was assumed by previous studies is not a good assumption [8, 32]. Figs. 12 and 13 show the effect of various feed flow rates (0.5, 1 and 1.5 l/min) on water concentration along the z and r directions, respectively. At greater values of feed flow rate, water concentration values are greater (at the same radius or dimensionless height). This is because an increase in feed flow rate, diminishes the contact time of feed flow with membrane, thus less water has enough time to pass through the membrane. This is in good agreement with what is expected in real conditions.

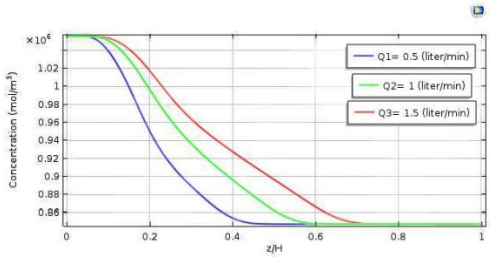

Fig.12 *Water concentration distribution vs. dimensionless height in feed phase at 30°C temperature and various feed flow rates*

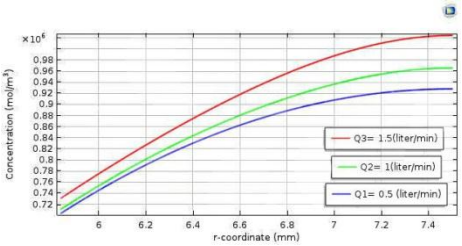

Fig.13 *Water concentration distribution in feed phase vs. radius at 30°C temperature and various feed flow rates*

4.3. Water concentration distribution in membrane phase

Fig. 14 shows the concentration distribution of water in membrane phase at different separation times.

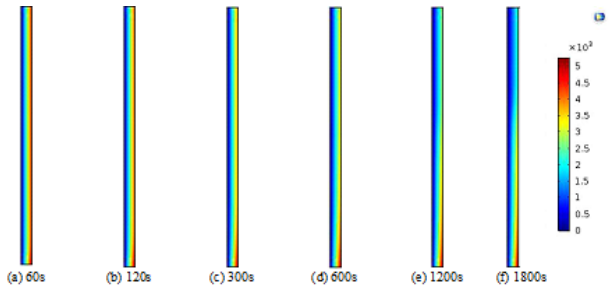

Fig. 14 *Concentration distribution of water in membrane phase ($C_{water\text{-}membrane}$) at different separation times (1 l/min flow rate and 30°C temperature); (a) 60s, (b) 120s, (c) 300s, (d) 600s, (e) 1200s and (f) 1800s*

Water transfer through the membrane was described only by diffusion mechanism. Since at the membrane-permeate interface the vacuum condition was assumed, the water concentration on this boundary is zero at all separation times. At the beginning of the separation process (times less than 300s) the water concentration on the membrane-feed interface is greater. This is because the water concentration on this boundary is calculated from its value in the feed section, which is highest at the beginning of the separation process. Over a longer period of time however, water

concentration decreases on this boundary, especially in greater heights, due to the concentration decrease in feed side (as mentioned in the previous section). These results are very close to what happens in real conditions. Fig. 15 presents the water concentration in the membrane phase versus r-coordinate at different heights and times. As can be seen from the figure, water concentration increases with radius, as expected. Concentration value on the membrane-feed boundary ($r=R_2=5.835$mm) is maximum at any time, because it is calculated from water concentration in feed side, where its value is maximum. On the membrane-permeate interface, water concentration is zero because of vacuum applied in permeate side (dry membrane condition).

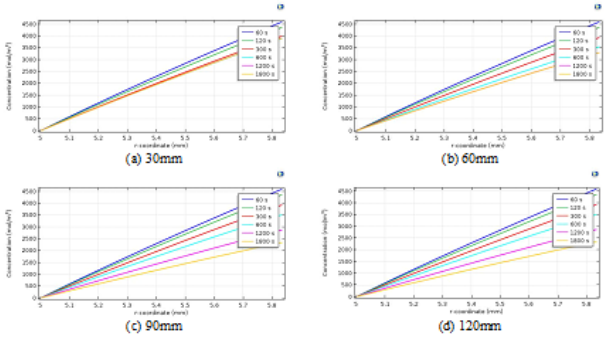

Fig. 15 *Concentration distribution of water in membrane phase ($C_{water\text{-}membrane}$) at different heights (1 l/min feed flow rate and 30°C temperature); (a) 30mm, (b) 60mm, (c) 90mm and (d) 120mm*

The concentration gradient at 5mm height differs slightly at different times. However, by increasing the height, concentration gradient becomes less over an extended period of time. This is because the model considers loss of concentration in greater heights and longer periods of time, due to more water transfer towards the membrane at regions near the feed inlet. As seen, the developed model powerfully is capable of predicting this mass loss at different membrane heights and separation times, which was neglected in previous studies [32]. Fig. 16 demonstrates the concentration distribution vs. dimensionless height at constant flow rate (1 l/min) and different membrane radii. Results show that the variation of water concentration along the z coordinate is considerable and cannot be neglected compared to its variation along r coordinate. Its variation is also greater over an extended period of time, as expected. The total shape of concentration distribution is almost the same at various radii. However, at radii far from the membrane-permeate interface, the concentration increases considerably. This is because water concentration on the membrane-feed interface is calculated from selectivity equation (Eq. 1) and water concentration in feed phase, where its value is highest.

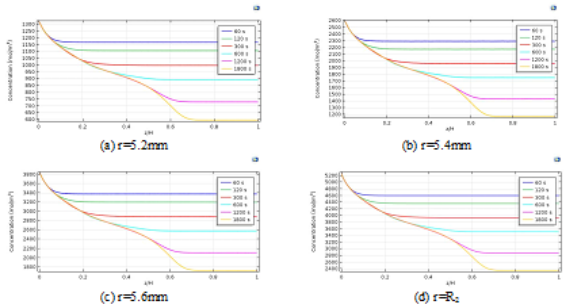

Fig. 16 *Concentration distribution of water in membrane phase ($C_{water\text{-}membrane}$) vs. dimensionless heights at different radii (1 l/min flow rate and 30°C temperature); (a) r=5.2mm, (b) r=5.4mm, (c) r=5.6mm and (d) $r=R_2$*

Figs 17 and 18 show the effect of various feed flow rates (0.5, 1 and 1.5 l/min) on water concentration along the z and r coordinates, respectively. As can be seen from the figures, water concentration is higher at greater flow rates. This is because an increase in feed flow rate diminishes the contact time of feed flow with membrane. Thus higher concentrations are achieved in the feed phase and consequently in the membrane. However, concentration slightly increases with flow rate at different radii. This indicates that flow rate has negligible effect on concentration distribution along r direction.

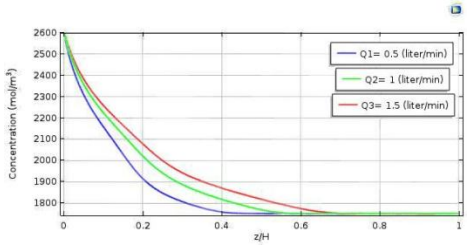

Fig. 17 *Concentration distribution of water in membrane phase ($C_{water\text{-}membrane}$) vs. dimensionless height at different feed flow rates*

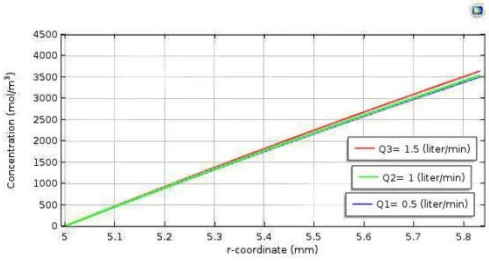

Fig. 18 *Concentration distribution of water in membrane phase ($C_{water\text{-}membrane}$) vs. radius at different feed flow rates*

4.4. Velocity distribution in feed phase

Fig. 19 shows the velocity field in the feed phase of the PV membrane system. The velocity distribution was obtained using numerical solution of momentum balance. This was done by adding a "laminar flow" physic to the whole model in COMSOL. As can be seen from the figure, the velocity magnitude is highest at the feed inlet, where the velocity has maximum value. Velocity is zero on the membrane-feed interface and at membrane height due to no slip conditions assumed on these boundaries. Thus the velocity magnitude is almost zero at heights more than 30 mm.

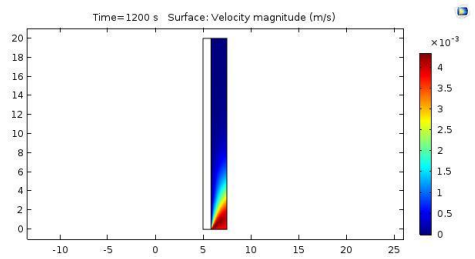

Fig. 19 *Velocity distribution in the feed phase at 1 l/min feed flow rate and 30°C temperature*

5. Conclusion

Nano pore Mordenite membranes were firstly used for dehydration of water-UDMH mixtures. The membranes were synthesized on the outer surface of porous mullite tubes by hydrothermal method. The mullite supports were made by extruding kaolin clay. Zeolite membranes showed much higher fluxes and separation factors than commercially available polymeric membranes. The membranes showed good membrane performance for separation of the UDMH-water mixtures. It is expected that even significantly higher fluxes, with similar separation factors, can be achieved at higher temperatures. Since mordenite zeolite membranes can withstand high temperatures and harsh environments (pH>12), dehydration of the water-UDMH mixtures can be performed. It was found that PV using mordenite zeolite membranes is an effective technique to separate water from the water-UDMH mixtures. Finally, a comprehensive unsteady state model was developed to simulate water concentration distribution in feed and membrane phases with COMSOL Multiphysics software version 5.2. Navier-Stokes equations of mass and momentum transfer were solved in this software by finite element method (FEM). Effects of membrane length, membrane radius and feed flow rate were investigated. The results were very close to real conditions and indicated that FEM is an effective method for membrane separation modeling.

Nomenclature

C_{water}	water concentration (mol/m^3)
$C_{0,water}$	initial water concentration (mol/m^3)
$C_{water\text{-}feed}$	water concentration in feed (mol/m^3)
$C_{water\text{-}membrane}$	water concentration in membrane (mzol/m^3)
D_{water}	water diffusion coefficient (m^2/s)
$M_{embrane}$	water diffusion coefficient in membrane (m^2/s)
F	body force (N)
H	membrane height (mm)
n	partition coefficient
P	pressure (Pa)
P_{atm}	atmospheric pressure (Pa)
Q	flow rate (m^3/min)
r	radial coordinate
R_1	permeate-membrane radius (mm)
R_2	membrane-feed radius (mm)
R_3	feed outer radius (mm)
R	reaction term (mol/m^3.s)
S	selectivity
t	separation time (s)
U	velocity vector (m/s)
u	z-component velocity (m/s)
x_{UDMH}	UDMH wt.% in feed
x_{water}	water wt.% in feed
y_{UDMH}	UDMH wt.% in permeate
y_{water}	water wt.% in permeate
z	axial coordinate
ρ	density (kg/m^3)
μ	viscosity (Pa.s)

Refrences

[1]. Li, G., Kikuchi, E. and Matsukata, M., "The control of phase and orientation in zeolite membranes by the secondary growth method", Microporous and Mesoporous Materials, 62, 211, (2003).

[2]. Ravindra, R., Sridhar, S., Khan, A.A. and Rao, A.K., "Pervaporation of water, hydrazine and monomethylhydrazine using ethyl cellulose membranes", Polymer, 41, 2795 (2000).

[3]. Sridhar, S., Ravindra, R. and Khan, A.A., "Recovery of monomethylhydrazine liquid propellant by pervaporation technique", Ind. Eng. Chem. Res, 39(7), 2485 (2000).

[4]. Li, X.G., Kresse, I., Xu, Z.K. and Springer, J., "Effect of temperature and pressure on gas transport in ethyl cellulose membrane", Polymer, 42, 6801 (2001).

[5]. Ravindra, R., Krovvidi, K.R., Khan, A.A. and Rao, A.K., "D.S.C. studies of states of water, hydrazine and hydrazine hydrate in ethyl cellulose membrane", Polymer, 40, 1159 (1999).

[6]. Ravindra, R., Kameswara, A. and Khan, A., "A qualitative evaluation of water and monomethyl hydrazine in ethyl cellulose membrane", Journal of Applied Polymer Science, 72, 689 (1999).

[7]. Hu, S., Ren, W., Cai, D., Hughes, T.C., Qin, P. and Tan, T., "A mixed matrix membrane for butanol pervaporation based on micron-sized silicalite-1 as macro-crosslinkers", Journal of Membrane Science, 533, 270 (2017).

[8]. Moullik, S., Kumar, K.P., Bohra, S. and Sridhar, S., "Pervaporation performance of PPO membranes in dehydration of highly hazardous MMH and UDMH liquid propellants", Journal of Hazardous Materials, 288, 69 (2015).

[9]. Ramaiah, K.P., Satyasri, D., Sridhar, S. and Krishnaiah, A., "Removal of hazardous chlorinated VOCs from aqueous solutions using novel ZSM-5 loaded PDMS/PVDF composite membrane consisting of three hydrophobic layers", Journal of Hazardous Materials, 261, 362 (2013).

[10]. Wang, Q., Li, N., Bolto, B., Hoang, M. and Xie, Z., "Desalination by pervaporation: A review", Desalination, 387, 46 (2016).

[11]. Li, J., Wang, N., Yan, H., Zhang, G., Qin, Z., Ji, S. and Zhang, G., "Roll-coating of defect-free membranes with thin selective layer for alcohol permselective pervaporation: From laboratory scale to pilot scale", Chemical Engineering Journal, 289, 106 (2016).

[12]. Liao, Y.L., Hu, C.C., Lai, J.Y. and Liu, Y.L., "Crosslinked polybenzoxazine based membrane exhibiting in-situ self-promoted separation

performance for pervaporation dehydration on isopropanol aqueous solutions", Journal of Membrane Science, 531, 10 (2017).

[13]. Xu, Y.M. and Chung, T.S., "High-performance UiO-66/polymide mixed matrix membranes for ethanol, isopropanol and n-butanol dehydration via pervaporation", Journal of membrane Science, 531, 16 (2017).

[14]. Yong, W.F., Salehian, P., Zhang, L. and Chung, T.S., "Effects of hydrolyzed PIM-1 in polymide-based membranes on C_2-C_4 alcohols dehydration via pervaporation", Journal of Membrane Science, 523, 430 (2017).

[15]. Xu, Y.M., Le, N.L., Zuo, J. and Chung, T.S., "Aromatic polymide and crosslinked thermally rearranged poly (benzoxazole-co-imide) membranes for isopropanol dehydration via pervaporation", Journal of Membrane Science, 499, 317 (2016).

[16]. Amirilargani, M. and Sadatnia, B., "Poly (vinyl alcohol)/zeolitic imidazolate frameworks (ZIF-8) mixed matrix membranes for pervaporation dehydration of isopropanol", Journal of Membrane Science, 469, 1 (2014).

[17]. Amirilargani, M., Ghadimi, A., Tofighy, M.A. and Mohammadi, T., "Effects of poly (allylamine hydrochloride) as a new functionalization agent for preparation of poly vinyl alcohol/multiwalled carbon nanotubes membranes", Journal of Membrane Science, 447, 315 (2013).

[18]. Zhao, J., Wang, F., Pan, F., Zhang, M., Yang, X., Li, P., Jiang, Z., Zhang, P., Cao, X. and Wang, B., "Enhanced pervaporation dehydration performance of ultrathin hybrid membrane by incorporating bioinspired multifunctional modifier and $TiCl_4$ into chitosan", Journal of Membrane Science, 446, 395 (2013).

[19]. Fathizadeh, M., Aroujalian, A., Raisi, A. and Fotouhi, M., "Preparation and characterization of thin film nanocomposite membrane for pervaporation dehydration of aqueous alcohol solutions", Desalination, 314, 20 (2013).

[20]. Mosleh, S., Khosravi, T., Bakhtiari, O. and Mohammadi, T., "Zeolite filled polymide membranes for dehydration of isopropanol through pervaporation process", Chemical Engineering Research and Design, 90(3), 433 (2012).

[21]. Widjojo, N. and Chung, T.S., "Pervaporation dehydration of C_2-C_4 alcohols by 6FDA-ODA-NDA/Ultem dual-layer hollow fiber membranes with enhanced separation performance and swelling resistance", Chemical Engineering Journal, 155(3), 736 (2009).

[22]. Samei, M., Iravaninia, M., Mohammadi, T. and Asadi, A.A., "Solution diffusion modeling of a composite PVA/fumed silica ceramic supported membrane", Chemical Engineering and Processing: Process Intensification, 109, 11 (2016).

[23]. Sridhar, S., Susheela, G., Reddy, G.J. and Khan, A.A., "Cross linked chitosan membranes: characterization and study of dimethylhydrazine dehydration by pervaporation", Polymer International, 50, 1156 (2001).

[24]. Ravindra, R., Rao, A.K. and Khan, A.A., "Processing of liquid propellant reaction liquors by pervaporation", Journal of Applied Polymer Science, 72, 141 (1999).

[25]. Ravindra, R., Sridhar, S. and Khan, A.A. "Separation studies of hydrazine from aqueous solutions by Pervaporation", Journal of Polymer Science: Part B: Polymer Physics, 37(16), 1969 (1999).

[26]. Ravindra, R., Krovvidi, R. and Khan, A., "Solubility parameter of chitin and chitosan", Carbohydrate Polymers, 36(2-3), 121 (1998).

[27]. Li, G., Kikuchi, E. and Matsukata, M., "A study on the pervaporation of water–acetic acid mixtures through ZSM-5 zeolite membranes", Journal of Membrane Science, 218(1-2), 185 (2003).

[28]. Zhang, Y., Xub, Z. and Chenb, Q., "Synthesis of small crystal polycrystalline mordenite membrane", Journal of Membrane Science, 210, 361 (2002).

[29]. Navajas, A., Mallada, R., Tellez, C., Coronas, J., Menhdez, M. and Santamaria, J., "Preparation of mordenite membranes for pervaporation of water-ethanol mixtures", Desalination, 148, 25 (2002).

[30]. Casado, L., Mallada, R., Téllez, C., Coronas, J., Menéndez, M. and Santamaría, J., "Preparation, characterization and pervaporation performance of mordenite membranes", Journal of Membrane Science, 216, 135 (2003).

[31]. Piera, E., Salomón, M.A., Coronas, J., Menéndez, M. and Santamaría, J., "Synthesis, characterization and separation properties of a composite mordenite/ZSM-5/chabazite hydrophilic membrane", Journal of Membrane Science, 149, 99 (1998).

[32]. Rezakazemi, M., Shahverdi, M., Shirazian, S., Mohammadi, T. and Pak, A., "CFD simulation of water removal from water/ethylene glycol mixtures by pervaporation", Chemical Engineering Journal, 168, 60 (2011).

[33]. Rom, A., Miltner, A., Wukovits, W. and Friedl, A., "Energy saving potential of hybrid membrane and distillation process in butanol purification: Experiments, modeling and simulation", Chemical Engineering and Processing, 104, 201 (2016).

[34]. Liu, D., Liu, G., Meng, L., Dong, Z., Huang, K. and Jin, W., "Hollow fiber modules with ceramic-supported PDMS composite membranes for pervaporation recovery of bio-butanol", Separation and Purification Technology, 146, 24 (2015).

[35]. Jain, M., Attarde, D. and Gupta, S.K., "Removal of thiophenes from FCC gasoline by using a hollow fiber pervaporation module: Modeling, validation and influence of module dimensions and flow directions", Chemical Engineering Journal, 308, 632 (2017).

[36]. Moulik, S., Nazia, S., Vani, B. and Sridhar, S., "Pervaporation separation of acetic acid/water mixtures through sodium alginate/polyaniline polyion complex membrane", Separation and Purification Technology, 170, 30 (2016).

[37]. Qiao, Z., Wu, Y., Li, X. and Zhou, J., "Molecular simulation on the separation of water/ethanol azeotropic mixture by poly(vinyl alcohol) membrane", Fluid Phase Equilibria, 302, 14 (2011).

[38]. Qu, H., Kong, Y., Lv, H., Zhang, Y., Yang, J. and Shi, D., "Effect of crosslinking on sorption, diffusion and pervaporation of gasoline components in hydroxyethyl cellulose membranes", Chemical Engineering Journal, 157(1), 60 (2010).

[39]. Lin, L., Zhang, Y. and Kong, Y., "Pervaporation separation of n-heptane-thiophene mixtures by polyethylene glycol membranes: Modeling and experimental", Journal of Colloid and Interface Science, 339(1), 152 (2009).

[40]. Das, P. and Ray, S.K., "Analysis of sorption and permeation of acetic acid-water mixtures through unfilled and filled blend membranes", Separation and Purification Technology, 116, 433 (2013).

[41]. Das, P. and Ray, S.K., "Pervaporation recovery of tetrahydrofuran from water with plasticized and filled polyvinylchloride membranes", Journal of Industrial and Engineering Chemistry, 34, 321 (2016).

[42]. Kazemimoghadam, M., Pak, A. and Mohammadi, T., "Dehydration of water/1-1-dimethylhydrazine mixtures by zeolite membranes", Microporous and mesoporous materials, 70(1), 127 (2004).

[43]. Li, G., Kikuchi, E. and Matsukata, M., "Separation of water_acetic acid mixtures by pervaporation using a thin mordenite membrane", Separation and Purification Technology, 32(1-3), 199 (2003).

[44]. Bird, R.B., Stewart, W.E. and Lightfoot, E.N., "Transport phenomena", Second ed., John Wiley & Sons, New York, USA, p. 780 (1960).

[45]. Rezakazemi, M., Niazi, Z., Mirfendereski, M., Shirazian, S., Mohammadi, T. and Pak, A., "CFD simulation of natural gas sweetening in a gas-liquid hollow-fiber membrane contactor", Chemical Engineering Journal, 168, 1217 (2011).

[46]. Zourmand, Z., Faridirad, F., Kasiri, N. and Mohammadi, T., "Mass transfer modeling of desalination through an electrodialysis cell", Desalination, 359, 41 (2015).